SCIENTIFIC ARTICLE

Quantitative 3-Dimensional CT Analyses of Intramedullary Headless Screw Fixation for Metacarpal Neck Fractures

Paul W. L. ten Berg, MSc, Chaitanya S. Mudgal, MD, Matthew I. Leibman, MD, Mark R. Belsky, MD, David E. Ruchelsman, MD

Purpose Fixation countersunk beneath the articular surface is well accepted for periarticular fractures. Limited open intramedullary headless compression screw (HCS) fixation offers clinical advantages over Kirschner wire and open techniques. We used quantitative 3-dimensional computed tomography to assess the articular starting point, surface area, and subchondral volumes used during HCS fixation of metacarpal neck fractures.

Methods We simulated retrograde intramedullary insertion of 2.4- and 3.0-mm HCS and 1.1-mm Kirschner wires for metacarpal neck fracture fixation in 3-dimensional models from 16 adults. We used metacarpal head articular surface area (mm^2) and subchondral volumes (mm^3) and coronal and sagittal plane arcs of motion, during which we analyzed the center and rim of the articular base of the proximal phalanx engaging the countersunk entry site.

Results Mean metacarpal head surface area mated to the proximal phalangeal base in neutral position was 93 mm^2; through the coronal plane arc (45°), 129 mm^2, and through the sagittal plane arc (120°), 265 mm^2. The mean articular surface area used by countersunk HCS threads was 12%, 8%, and 4%, respectively, in each of these arcs. The 1.1-mm Kirschner wire occupied 1.2%, 0.9%, and 0.4%, respectively. Mean metacarpal head volume was 927 mm^3. Mean subchondral volume occupied by the countersunk portion was 4%. The phalangeal base did not overlap the dorsally located countersunk entry site through most of the sagittal plane arc. During coronal plane motion in neutral extension, the center of the base never engaged the dorsally located countersunk entry site.

Conclusions Metacarpal head surface area and subchondral head volume occupied by HCS were minimal. Articular surface area violation was least during the more clinically relevant sagittal plane arc of motion.

Clinical relevance The dorsal articular starting point was in line with the medullary canal, and avoided engaging the center of the articular base through most of the sagittal plane arc. Three-dimensional computed tomography data support the use of an articular starting point for these extra-articular fractures. *(J Hand Surg 2013;xx:. Copyright © 2013 by the American Society for Surgery of the Hand. All rights reserved.)*

Key words Hand fracture, headless screw, intramedullary fixation, metacarpal neck.

Additional material is available online.

From the Hand and Upper Extremity Surgery Service, Massachusetts General Hospital/Harvard Medical School, Boston; and Hand Surgery, P.C., Newton-Wellesley Hospital/Tufts University School of Medicine, Newton, MA; and the Academic Medical Center, Amsterdam Zuidoost, The Netherlands.

Received for publication April 18, 2012; accepted in revised form September 26, 2012.

No benefits in any form have been received or will be received related directly or indirectly to the subject of this article.

Corresponding author: David E. Ruchelsman, MD, Hand Surgery, P.C., Newton-Wellesley Hospital, 2000 Washington Street, Blue Building, Suite 201, Newton, MA 02462; e-mail: druchelsman@partners.org.

0363-5023/13/xx0x-0001$36.00/0
http://dx.doi.org/10.1016/j.jhsa.2012.09.029

Fixation countersunk beneath the articular surface is well accepted for various upper extremity fractures.[1–8] We have previously described limited-open retrograde intramedually cannulated headless screw fixation of metacarpal neck–subcapital fractures[9] and have increasing clinical experience with this technique. Multiple fixation techniques for displaced and markedly angulated metacarpal neck and subcapital fractures and axially stable shaft fractures have been described, including percutaneous and limited open antegrade (ie, bouquet pinning),[10] retrograde (ie, longitudinal intramedullary fixation),[11] transmetacarpal Kirschner wire constructs,[12] and plate fixation.[13] Each technique has its own advantages and disadvantages. There is no consensus on an optimal treatment modality.[13]

Retrograde intramedullary fixation using a cannulated headless screw can be achieved using a limited-open extensor-splitting approach and represents only 1 additional step beyond longitudinal intramedullary retrograde Kirschner wire fixation of these fractures through the metacarpal head articular surface. The headless design allows fixation to be countersunk beneath the articular surface and allows for early postoperative joint motion.[14] Potentially, direct visualization of the starting point also eliminates multiple attempts to achieve the correct starting point during percutaneous Kirschner wire insertion for retrograde intramedullary fixation.

Traditionally, the use of headless screws has been reserved for fixation of articular and complex periarticular fractures.[1–8] The long-term impact of articular insertion starting points for subchondral headless screw fixation has not been fully elucidated for articular–periarticular and extra-articular fractures. Our group has previously used quantitative 3-dimensional computed tomography (CT) techniques to better define articular fracture characteristics.[15–19] Simulation of retrograde headless screw intramedullary fixation of metacarpal neck and subcapital fractures in 3-dimensional CT–generated models may help improve our understanding of the magnitude of articular surface area (SA) and subchondral volume (SCV) used with this technique, characteristics helpful in optimizing implant design and fixation techniques in periarticular fractures. In addition, during simulated arcs of metacarpophalangeal (MCP) joint motion in the coronal and sagittal planes, we assessed the degree of engagement of the entry site of the countersunk screw with the base of proximal phalanx.

MATERIALS AND METHODS

Inclusion and exclusion criteria

From a list of CT scans of the hand obtained from our Division of Musculoskeletal Radiology, we identified 16 CT scans of the hand with a slice thickness of 0.62 mm that included intact MCP joints of the ring and little fingers for 3-dimensional modeling. We used several CT scanners with up to 140 KV and 500 to 700 mAs and with slices from 8 to 64/dual source. We used scans from 8 men and 8 women with a mean age of 45 years (SD, 17 y; range, 21–74 y). We limited the number to 16 because the analysis techniques were time and resource intensive. Our institution's human research committee approved this protocol.

Modeling technique

Our technique has previously been described in detail.[15] We obtained Digital Imaging and Communications in Medicine files of CT slices through Vitrea (Vitrea 2 software; Vital Images, Plymouth, MN) and exported them for further processing into MATLAB (version 7.7; The MathWorks, Natick, MA) to identify higher densities (bone structures). These images were then uploaded into Rhinoceros (version 4.0; McNeel North America, Seattle, WA). We used a specialized code written by the Massachusetts General Hospital (Boston, MA) 3D Imaging Service to account for pixel size and distance between CT slices during conversion of the Vitrea Digital Imaging and Communications in Medicine images into Rhinoceros Joint Photographic Experts Group files. In this latter architecture software, the images were stacked with pointwise representation of the bone. This modeling technique then used lines between each point to create hollow 3-dimensional models from CT slices based on the wire model of the cortical bone. With this technique, we created a total of 32 3-dimensional models of ring and little metacarpals.

Based on our clinical experience with intramedullary 2.4- and 3.0-mm headless compression screw (HCS) fixation (Synthes, Paoli, PA) for metacarpal subcapital and neck fractures, we used the dimensions of these headless compression screws to create 3-dimensional screws in each metacarpal head–neck model. The 2.4- and 3.0-mm HCS have head diameters of 3.1 and 3.5 mm (trailing threads), shaft diameters of 2.0 mm, and a leading thread diameter of 2.4 and 3.0 mm, respectively. Both screws have a trailing thread length of 2 mm.

Metacarpal head articular surface area and volumetric analyses

In the first phase, we defined the metacarpal head SA mated by the phalangeal positions in neutral position (0°), throughout the sagittal (120°) and coronal (45°) plane arcs of motion. The proximal phalanges were initially sequentially positioned from −30° hyperexten-

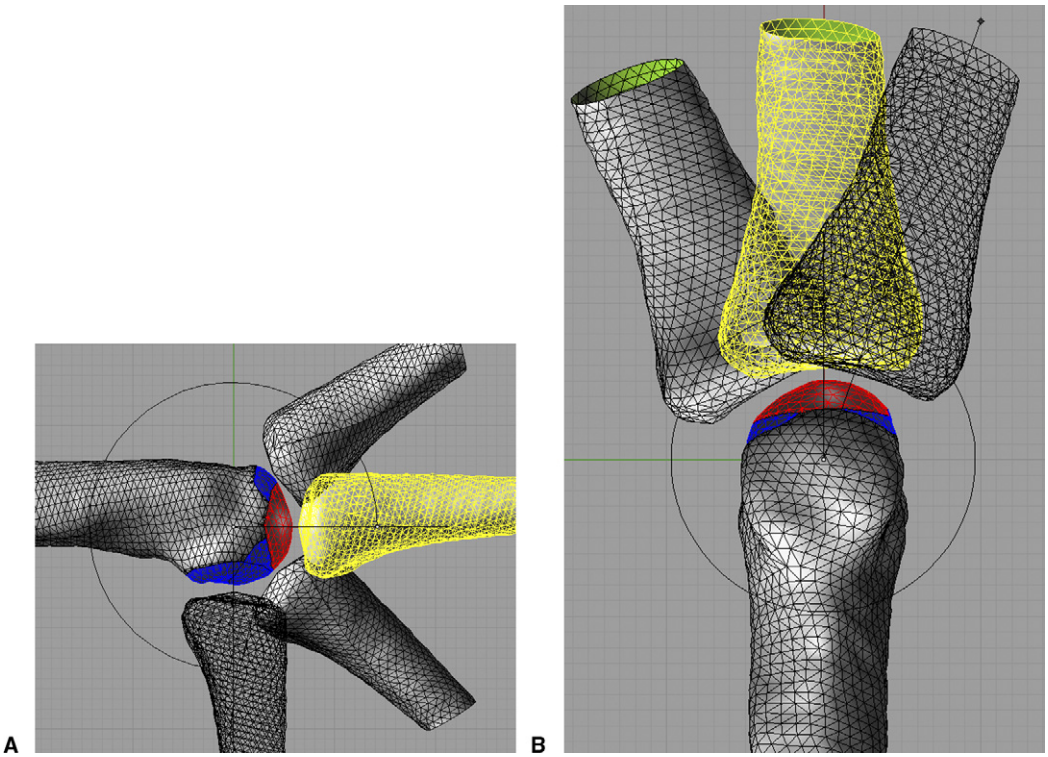

FIGURE 1: A Lateral view of the 120° maximal arc of sagittal plane motion: 30° hyperextension to 90° flexion. In both **A** and **B** the red area on the metacarpal head is the articular surface mated with the phalangeal base in neutral extension 0° (yellow phalanx). The blue area is the additional articular surface mated by the phalangeal base in (hyper)extension, midflexion, and maximal flexion. **B** Dorsal view of the 45° maximal arc of coronal plane motion: 25° abduction (left phalanx) to +20° adduction (right phalanx). The blue area is the additional articular surface mated by the phalangeal base in maximal abduction and adduction.

sion to 90° flexion to visualize the maximal hyperextension-flexion range of active MCP joint motion relative to the longitudinal phalangeal axis in the sagittal plane. We defined midflexion as 45° to model a smooth transition from neutral extension (ie, 0°) to 90° flexion (Fig. 1). In neutral extension (0°), we then positioned the proximal phalanges from 25° abduction to 20° adduction to visualize the maximal abduction-adduction range of motion in the coronal plane (Fig. 1). In the coronal and sagittal planes, the center of the metacarpal head was defined as the axis of rotation.

We visualized the articular SA of the metacarpal heads in contact with the fourth and fifth proximal phalanges using a feature called surface angle analysis. We estimated the metacarpal head articular SA mated by the phalangeal positions throughout the sagittal (120°) and coronal (45°) plane arcs of motion (Fig. 1) by sequentially overlapping the phalanx in line with its longitudinal axis on the metacarpal head (Fig. 2).

In the second phase, we analyzed the consequences of the HCS insertions: the magnitude of violation of the articular SA and of the SCV and, during simulated arcs of joint motion, the degree of engagement of the entry site of the countersunk screw with the base of proximal phalanx. We placed the screws retrograde and countersunk them beneath the articular surface along the dorsal corridor of the metacarpal head, which is offset from the neck and in line with the medullary canal (Figs. 3, 4). We created the buried trailing portion of the HCS by making a cylinder with the same diameter as the head of the HCS and with the same outer SA as the metacarpal head. We then calculated articular SA violation of the metacarpal head for each HCS. We then compared surface area used by this technique with that of retrograde intramedullary 1.1-mm Kirschner wire fixation, a common percutaneous technique used for these fractures. To calculate the articular SA violation of the metacarpal head by a Kirschner wire with a diameter of 1.1 mm, we reduced the diameter of the countersunk cylinders to 1.1 mm in each metacarpal head–neck model.

To analyze the SCV of the metacarpal head, we positioned a cutting plane with a 2-dimensional curve along the anatomical transition from the metacarpal shaft to the head–neck region. This plane allowed for

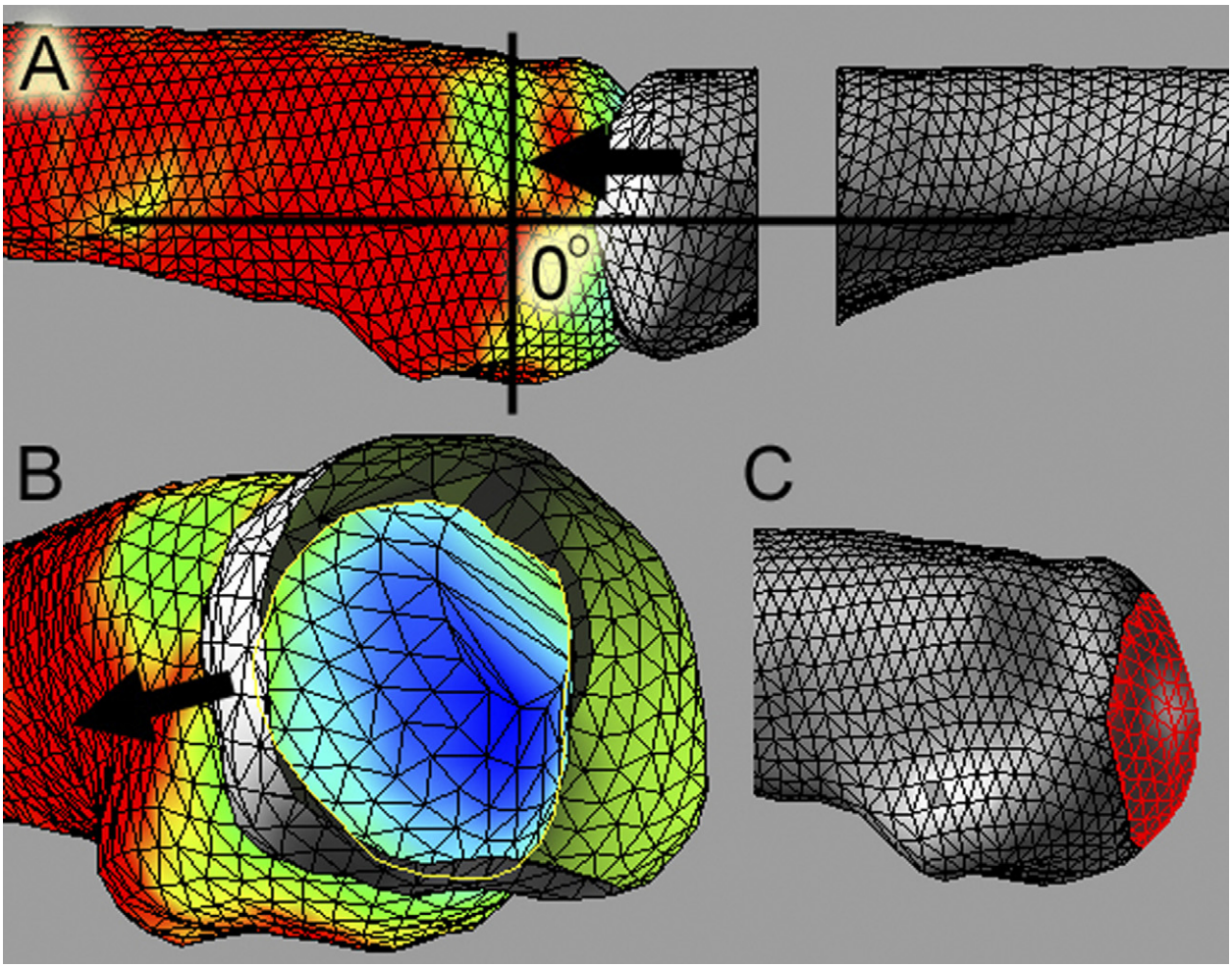

FIGURE 2: The articular surface area on the metacarpal head mated by the surface of the proximal phalangeal base in neutral position of 0° can be estimated by shifting the phalangeal base in line with its longitudinal axis onto the metacarpal head (model A), until all angles within 70° to 90° of orthogonal are included (model B). Subsequently, an intersection between both metacarpal and phalangeal surface can separate this specific articular surface (red area) (model C). This technique is applicable to all phalangeal positions. The articular surfaces mated by the different phalangeal positions can be projected onto the same metacarpal head as in Figure 1.

analysis of the SCV occupied by the headless segment of the screw and its trailing threads (Fig. 3).

We calculated the arc of motion during which the center of the articular base of the proximal phalanx engaged the entry site (ES) of the countersinking screw in the coronal and sagittal planes (Fig. 4A). In addition, we also assessed the arc during which there is no contact between the base of the phalanx and ES (ie, the phalangeal base did not obscure the ES of the head of the screw) (Fig. 4B).

RESULTS

Table 1 lists the mean magnitude of metacarpal head SA engaged by the proximal phalangeal base in neutral position. Surface area analyses demonstrated that the ES constituted variable percentages of the articular surface proportionate to the size of the implant (Table 2). The absolute violations of the metacarpal head SA by the 2.4-mm screw, 3.0-mm screw, and 1.1-mm Kirschner were 9, 12, and 1 mm^2, on average.

The mean SCV of the metacarpal heads of the ring and little fingers were 1,050 mm^3 (SD, 187 mm^3; range, 711–1,280 mm^3) and 802 mm^3 (SD, 141 mm^3; range, 466–992 mm^3), respectively. On average, the countersunk trailing portion of the 2.4- and 3.0-mm HSC occupied 4% and 5% of head SCV, respectively.

The rim of the phalangeal base did not overlap the countersunk ES in 64% of the 120° sagittal plane arc modeled. The center of the phalangeal base was unengaged in 87% of the hyperextension–flexion arc. During coronal plane motion in neutral extension of 0°, the rim of the phalangeal base over-

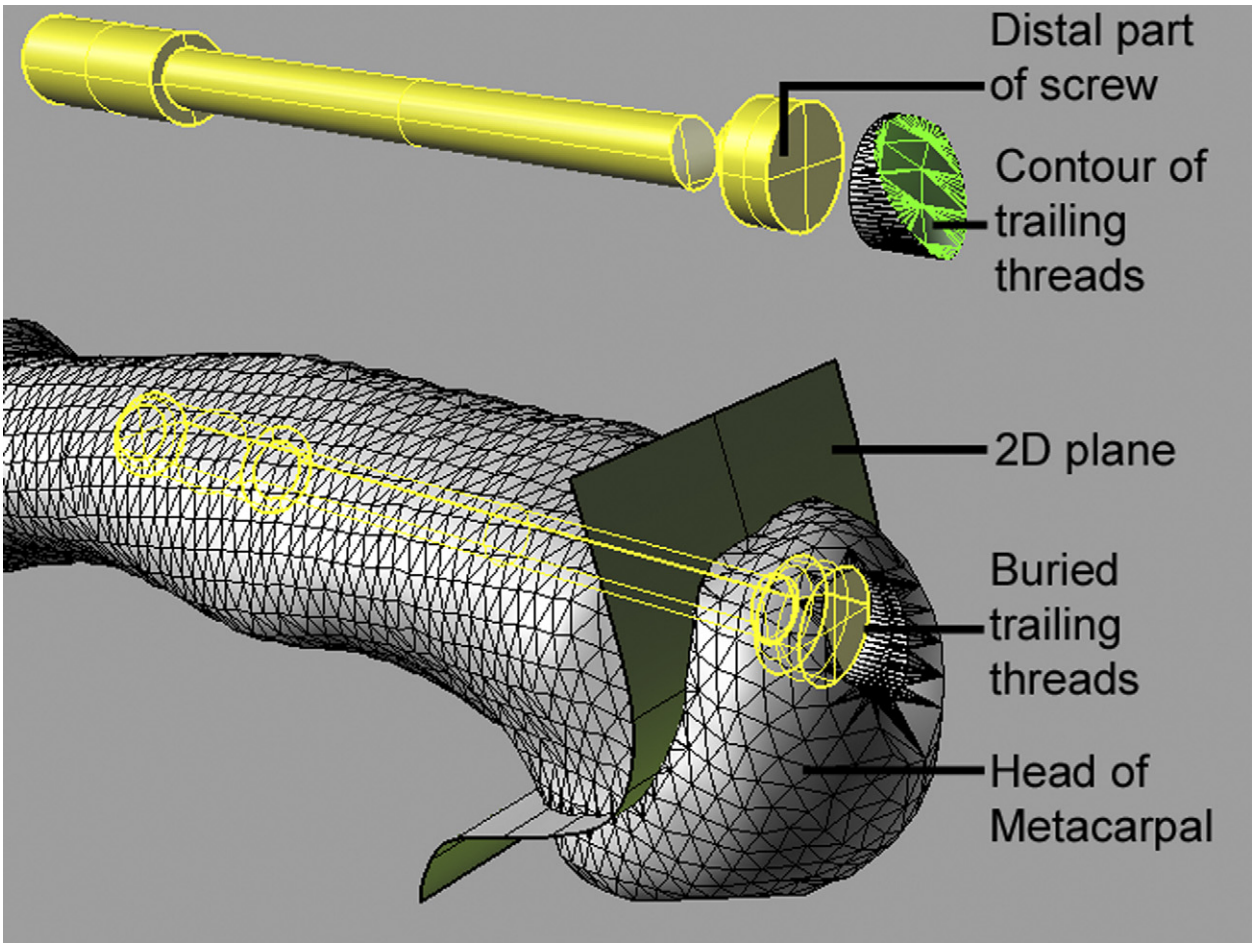

FIGURE 3: A 2-dimensional cutting plane is placed at the anatomical transition between shaft and head–neck. Surface area (green) and volumetric analyses of the cylindrical zone of the buried trailing threads are performed.

lapped the countersunk ES during the entire 45° abduction–adduction arc. However, the center of the base never engaged the dorsally located countersunk ES (see Appendices A and B, available on the Journal's Web site at www.jhandsurg.org).

DISCUSSION

Various fixation techniques[10–13] have been described for the reduction and stabilization of displaced and markedly angulated metacarpal neck and subcapital fractures. Selection of technique is often based on fracture characteristics and surgeon preference. Although percutaneous Kirschner wire techniques limit soft tissue dissection, 3 to 4 weeks of postoperative immobilization are required to minimize the risk of superficial and deep pin track infections, which may necessitate early Kirschner wire removal and additional procedures.

Kirschner wires left in place may be cut and buried beneath the skin or left protruding through the skin where the tip is bent.[20] Two large series[21,22] reported a similar overall complication rate (16%) after percutaneous Kirschner wire fixation of various hand and wrist fractures. Major complications included osteomyelitis, tendon rupture, nerve injury, and pin track infection. Pin track infection rates were similar in both series (6%[21] and 5%[22]). Buried Kirschner wires may reduce the incidence of infection[23–25] but potentially increase the risk of a tendon rupture[26] or necessitate return to the operating room for removal.[24]

In contrast, formal open reduction and internal fixation may achieve rigid fixation and facilitate early postoperative rehabilitation, but complications are well described.[27,28] In a series of 129 patients with 157 metacarpal fractures treated by open reduction and internal plate fixation, Fusetti et al[27] reported complications in more than one-third of the cohort, including delayed union, extensor adhesions and stiffness, fixation failure, complex regional pain syndrome, and deep infection. Page and Stern[28] found a similar major complication rate of 36% in 105 metacarpal and/or phalan-

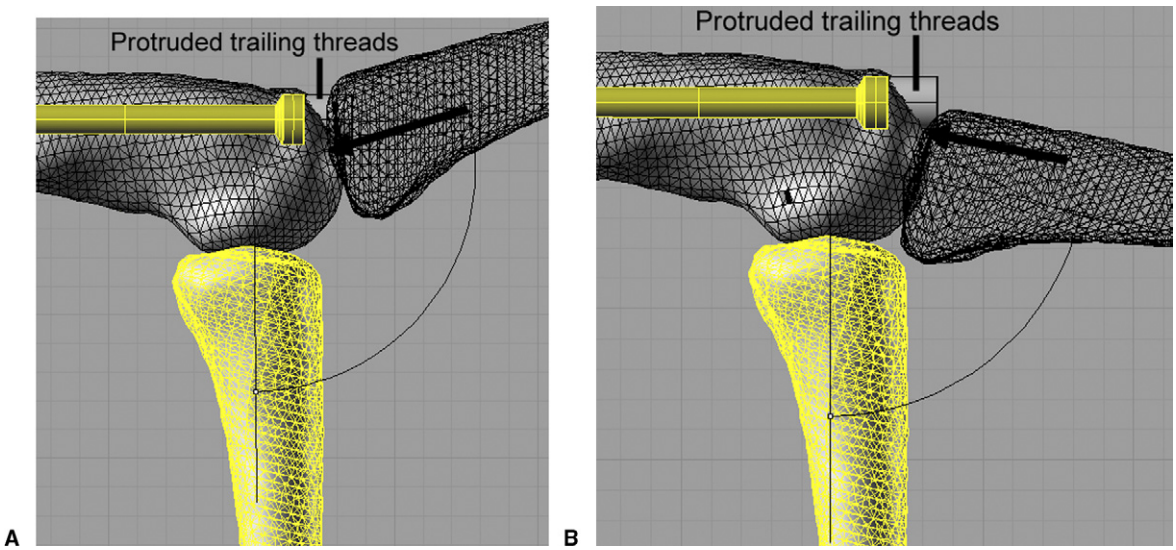

FIGURE 4: A Arc of motion in which the entry site of the trailing threads is not engaged by the center of the phalangeal base (black arrow). In the figure, the buried portion of the headless screw is protruded for a better view of the position of the entry site in lateral view. **B** Arc of motion in which the entry site of the trailing threads is not engaged by the rim of the phalangeal base (black arrow).

geal fractures stabilized with plates. Whereas newer precontoured angular-stable (ie, locking plates) plates available in customized configurations (ie, T, Y, L-shaped plates) may avoid the need to abut the dorsal articular margin for distal shaft– neck fractures, when there is limited distal bone stock and metaphyseal bone in subcapital fractures, often the plate needs to be placed to the level of the dorsal articular margin where the extensor mechanism is confluent with the dorsal capsule.

Optimal surgical fixation will limit surgical exposure of the fracture site, allow for early postoperative mobilization to regain full MCP joint motion and extensor excursion,[29] expedite return to activities of daily living and work or sport, and minimize the need for removal of hardware. Limited-open retrograde intramedullary headless screw fixation may achieve these goals and offers clinical advantages over Kirschner wire fixation and other open techniques.

Intramedullary headless screw fixation of subcapital metacarpal neck fractures with limited distal bone stock has previously been described.[9] We now have increasing clinical experience with this technique (Fig. 5) and have expanded our indications in select cases to include symptomatic nascent malunions and axial-stable transverse middiaphyseal fractures that are reducible with closed manipulation. Countersunk intramedullary fixation with isthmal purchase allows early active and active-assisted motion within the first postoperative week. A removable hand-based ulnar-gutter splint with the MCP joints in intrinsic plus position and the interphalangeal joints free is worn until suture removal and then is gradually weaned. This technique obviates concerns for pin track infections or adhesions after extensor tendon mobilization with formal open reduction and internal fixation. With neck comminution, the screw is inserted without the compression sleeve.

This technique is performed through a small split in the extensor tendon and a dorsal arthrotomy. Closed reduction is confirmed under fluoroscopic guidance, and a 1.1-mm Kirschner wire is then inserted under direct visualization for provisional fixation through the dorsal corridor in line with the medullary canal. It is then overdrilled and replaced with a 2.4- or 3.0-mm cannulated HCS based on preoperative templating of the dimensions of the isthmus of the intramedullary canal.

The use of HCS countersunk beneath the articular surface is well accepted for articular and complex periarticular fractures.[1–8] However, the impact of articular starting points for subchondral headless screw fixation has not been fully elucidated for articular and periarticular fracture patterns. Our simulations in 3-dimensional models showed relatively small values of violation of the metacarpal head surface area and subchondral metacarpal head volume with these headless screws. However, the violation of the metacarpal head SA by a 1.1-mm Kirschner wire is approximately 10-fold smaller, because a small difference in diameter of the fixation device has a relatively large impact on the articular SA.

TABLE 1. Mean Surface Area and Volume Measurements

	Men		Women		Men and Woman
	Ring	Small	Ring	Small	Ring and Small
Articular surface area (mm^2) by arc of motion					
Metacarpal C head neutral	102 (± 8; 89–113)	89 (± 11; 73–106)	93 (± 18; 65–125)	88 (± 6; 80–97)	93 (± 12; 65–125)
Metacarpal C head adduction-abduction	143 (± 8; 132–153)	123 (± 18; 103–148)	126 (± 24; 90–164)	125 (± 10; 109–136)	129 (± 17; 90–164)
Metacarpal C head flexion-(hyper) extension	302 (± 12; 281–317)	267 (± 26; 230–300)	256 (± 23; 225–286)	235 (± 23; 199–276)	265 (± 32; 199–317)
Volume metacarpal head (mm^3)	1200 (± 90; 1,090–1,280)	918 (± 39; 879–992)	902 (± 123; 71–1,100)	686 (± 101; 466–801)	927 (± 206; 466–1,280)

Three-dimensional CT surface analyses demonstrated that articular SA violation was least during the more clinically relevant maximal sagittal plane arc of active motion. The dorsal starting point was in line with the medullary canal and avoided engaging the center of the articular base of the phalanx through most of the sagittal plane arc. In neutral extension, the center of the base did not engage the countersunk entry site during the arc of abduction–adduction. Contraindications to this technique include subcapital–neck fractures with articular extension, fracture patterns that are axially unstable, open fractures with contamination of the medullary canal, and preexisting periarticular–diaphyseal deformity that precludes intramedullary screw fixation.

A relatively limited number of metacarpals (32 total: 16 male and 16 female) were modeled given the time-intensive nature of this modeling technique. We modeled ring and little finger metacarpals because these are the ones most commonly injured in clinical practice. Similar models for the index and middle finger can be created. Because their head size is larger, analysis of the ring and little finger yields worse case analyses with regard to impact on surface area and subchondral volume used. In our forthcoming clinical series of 30 metacarpal fractures treated with this technique, we treated only a single index finger metacarpal neck fracture. Modeling of the thumb would be more difficult given population variations in thumb MCP joint arcs of motion.

There is limited bias during construction of the 3-dimensional models, and a consistent algorithm for bone detection on CT slices and automated wire and 3-dimensional model creations is used.[16] A subjective aspect of the technique was defining the volume of the metacarpal head. However, the transition between the metacarpal shaft and head–neck junction was clearly visible in all cases and allowed for placement of the 2-dimensional cutting plane on the anatomical transition point. Surface angle analysis allowed reliable definition of the articular surface area without visualization of the articular cartilage on the CT images. Simulated screw insertion with accurate gridlines replicated intraoperative provisional Kirschner wire placement through the dorsal corridor of the metacarpal head, which is clearly visualized after fracture reduction, dorsal capsulotomy, and passive MCP flexion. Previous work by our group has demonstrated the utility of 3-dimensional CT modeling in upper extremity acute fractures.[15–19] Jung et al[30] used similar quantitative 3-dimensional CT techniques to define optimal headless screw position for scaphoid fixation.

Quantitative 3-dimensional CT analyses only support the use of an articular starting point for fixation of

TABLE 2. Mean Measurements in 8 Men and 8 Women in Ring and Little Finger After Screw Insertion

	Screw (2.4 mm)	Screw (3.0 mm)	Kirschner Wire (1.1 mm)
Surface violation			
SA metacarpal head neutral of 93 mm^2	10%	13%	1.2%
SA metacarpal head adduction-abduction of 129 mm^2	8%	9%	0.9%
SA metacarpal head flexion-(hyper)extension of 265 mm^2	4%	5%	0.4%
Volume violation			
Volume metacarpal head of 927 mm^3	4%	5%	
	Rim phalangeal base	Center phalangeal base	
Free motion without overlap countersunk			
120° sagittal plane arc of motion	64%	87%	
45° coronal plane arc of motion	0%	100%	

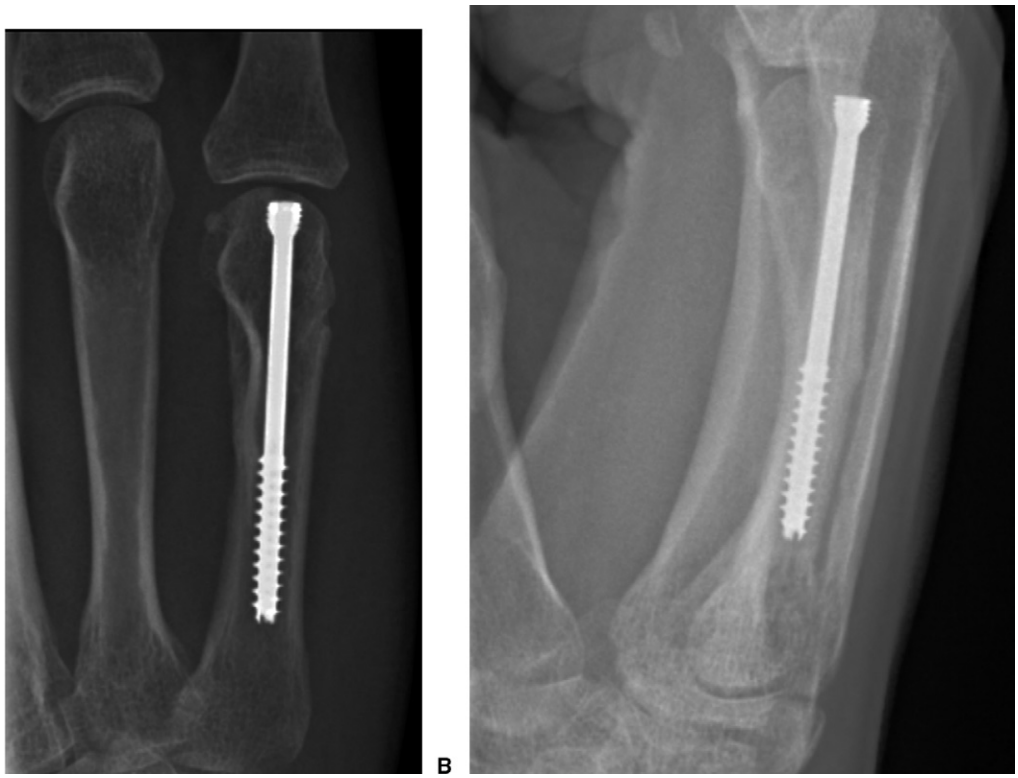

FIGURE 5: Intramedullary screw placement and radiographic union: **A** posteroanterior view, **B** lateral view. The patient recovered full active motion.

these fractures. Clinical results and outcomes data are needed to fully validate this technique. Further clinical investigation and outcomes research is ongoing to assess long-term clinical, functional, and radiographic outcomes with this technique. This study further highlights the utility of quantitative 3-dimensional CT analyses for assessing surgical techniques for acute fractures as well as posttraumatic reconstructive procedures. Data derived may have an impact on implant designs.

REFERENCES

1. Gereli A, Nalbantoglu U, Sener IU, Kocaoglu B, Turkmen M. Comparison of headless screws used in the treatment of proximal nonunion of scaphoid bone. *Int Orthop*. 2011;35(7):1031–1035.
2. Henry M. Variable pitch headless compression screw treatment of distal phalangeal nonunions. *Tech Hand Up Extrem Surg*. 2010;14(4):230–233.

3. Mighell M, Virani NA, Shannon R, Echols EL Jr, Badman BL, Keating CJ. Large coronal shear fractures of the capitellum and trochlea treated with headless compression screws. *J Shoulder Elbow Surg*. 2010;19(1):38–45.
4. Ruchelsman DE, Tejwani NC, Kwon YW, Egol KA. Open reduction and internal fixation of capitellar fractures with headless screws. *J Bone Joint Surg Am*. 2008;90(6):1321–1329.
5. Ruchelsman DE, Tejwani NC, Kwon YW, Egol KA. Open reduction and internal fixation of capitellar fractures with headless screws: surgical technique. *J Bone Joint Surg Am*. 2009;91(suppl 2):38–49.
6. Rutgers M, Mudgal CS, Shin R. Combined fractures of the distal radius and scaphoid. *J Hand Surg Eur Vol*. 2008;33(4):478–483.
7. Singisetti K, Aldlyami E, Middleton A. Early results of a new implant: 3.0 mm headless compression screw for scaphoid fracture fixation. *J Hand Surg Eur Vol*. 2012;37(7):690–693.
8. Slade JF III, Gillon T. Retrospective review of 234 scaphoid fractures and nonunions treated with arthroscopy for union and complications. *Scand J Surg*. 2008;97(4):280–289.
9. Boulton CL, Salzler M, Mudgal CS. Intramedullary cannulated headless screw fixation of a comminuted subcapital metacarpal fracture: case report. *J Hand Surg Am*. 2010;35(8):1260–1263.
10. Foucher G. "Bouquet" osteosynthesis in metacarpal neck fractures: a series of 66 patients. *J Hand Surg Am*. 1995;20(suppl 3):S86–S90.
11. Schadel-Hopfner M, Wild M, Windolf J, Linhart W. Antegrade intramedullary splinting or percutaneous retrograde crossed pinning for displaced neck fractures of the fifth metacarpal? *Arch Orthop Trauma Surg*. 2007;127(6):435–440.
12. Kozin SH, Thoder JJ, Lieberman G. Operative treatment of metacarpal and phalangeal shaft fractures. *J Am Acad Orthop Surg*. 2000;8(2):111–121.
13. Friedrich JB, Vedder NB. An evidence-based approach to metacarpal fractures. *Plast Reconstr Surg*. 2010;126(6):2205–2209.
14. Elkowitz SJ, Kubiak EN, Polatsch D, Cooper J, Kummer FJ, Koval KJ. Comparison of two headless screw designs for fixation of capitellum fractures. *Bull Hosp Jt Dis*. 2003;61(3-4):123–126.
15. Guitton TG, van der Werf HJ, Ring D. Quantitative three-dimensional computed tomography measurement of radial head fractures. *J Shoulder Elbow Surg*. 2010;19(7):973–977.
16. Guitton TG, van der Werf HJ, Ring D. Quantitative measurements of the volume and surface area of the radial head. *J Hand Surg Am*. 2010;35(3):457–463.
17. Guitton TG, Van Der Werf HJ, Ring D. Quantitative measurements of the coronoid in healthy adult patients. *J Hand Surg Am*. 2011; 36(2):232–237.
18. van Leeuwen DH, Guitton TG, Lambers K, Ring D. Quantitative measurement of radial head fracture location. *J Shoulder Elbow Surg*. 2012;21(8):1013–1017.
19. Guitton TG, Ring D. Three-dimensional computed tomographic imaging and modeling in the upper extremity. *Hand Clin*. 2010;26(3): 447–453.
20. Slone RM, Heare MM, Vander Griend RA, Montgomery WJ. Orthopedic fixation devices. *Radiographics*. 1991;11(5):823–847.
21. Hsu LP, Schwartz EG, Kalainov DM, Chen F, Makowiec RL. Complications of K-wire fixation in procedures involving the hand and wrist. *J Hand Surg Am*. 2011;36(4):610–616.
22. Stahl S, Schwartz O. Complications of K-wire fixation of fractures and dislocations in the hand and wrist. *Arch Orthop Trauma Surg*. 2001;121(9):527–530.
23. van Aaken J, Beaulieu JY, Della Santa D, Kibbel O, Fusetti C. High rate of complications associated with extrafocal kirschner wire pinning for distal radius fractures. *Chir Main*. 2008;27(4):160–166.
24. Hargreaves DG, Drew SJ, Eckersley R. Kirschner wire pin tract infection rates: a randomized controlled trial between percutaneous and buried wires. *J Hand Surg Br*. 2004;29(4):374–376.
25. Rafique A, Ghani S, Sadiq M, Siddiqui IA. Kirschner wire pin tract infection rates between percutaneous and buried wires in treating metacarpal and phalangeal fractures. *J Coll Physicians Surg Pak*. 2006;16(8):518–520.
26. Dowdy PA, Patterson SD, King GJ, Roth JH, Chess D. Intrafocal (Kapandji) pinning of unstable distal radius fractures: a preliminary report. *J Trauma*. 1996;40(2):194–198.
27. Fusetti C, Meyer H, Borisch N, Stern R, Santa DD, Papaloizos M. Complications of plate fixation in metacarpal fractures. *J Trauma*. 2002;52(3):535–539.
28. Page SM, Stern PJ. Complications and range of motion following plate fixation of metacarpal and phalangeal fractures. *J Hand Surg Am*. 1998;23(5):827–832.
29. McNemar TB, Howell JW, Chang E. Management of metacarpal fractures. *J Hand Ther*. 2003;16(2):143–151.
30. Jung WS, Jung JH, Chung US, Lee KH. Spatial measurement for safe placement of screws within the scaphoid using three-dimensional analysis. *J Plast Surg Hand Surg*. 2011;45(1):40–44.

APPENDIX A. Measurements in 8 Men

	Ring	Little
Surface		
A1. Countersunk for screw 2.4 (mm^2)	10 (± 2; 9–14)	9 (± 1; 9–11)
A2. Countersunk for screw 3.0 (mm^2)	12 (± 2; 11–16)	12 (± 1; 11–13)
B1. Articular surface metacarpal head neutral (mm^2)	102 (± 9; 89–113)	89 (± 11; 73–106)
A1/B2	10%	11%
A2/B1	12%	14%
B2. Articular surface metacarpal head adduction-abduction (mm^2)	143 (± 8; 132–153)	123 (± 18; 103–148)
A1/B2	7%	8%
A2/B2	8%	10%
B3. Articular surface metacarpal head flexion-(hyper)extension (mm^2)	302 (± 12; 281–317)	267 (± 26; 230–300)
A1/B3	3%	4%
A2/B3	4%	5%
Volume		
C1. Volume of countersunk portion of screw 2.4 (mm^3)	38 (± 4; 31–43)	35 (± 6; 28–41)
C2. Volume of countersunk portion of screw 3.0 (mm^3)	46 (± 5; 39–53)	42 (± 7; 33–50)
D. Volume of metacarpal head (mm^3)	1,200 (± 90; 1,090–1,280)	918 (± 39; 879–992)
C1/D	3%	4%
C2/D	4%	5%
Range of engagement phalanx—countersunk		
E1. Start of flexion range center of phalanx base (until 90° flexion)	−14 (± 3; −10 to −17)	−15 (± 1; −14 to 16)
Total extension-flexion range (120°)	86%	87%
E2. Start of flexion range rim of phalanx base (until 90° flexion)	14 (± 5; 7−21)	12 (± 1; 9−13)
Total extension-flexion range (120°)	63%	65%

APPENDIX B. Measurements in 8 Women

	Ring	Little
Surface		
A1. Countersunk for screw 2.4 (mm^2)	9 (± 1; 9−10)	9 (± 1; 9−10)
A2. Countersunk for screw 3.0 (mm^2)	12 (± 1; 11−13)	12 (± 1; 11−13)
B1. Articular surface metacarpal head neutral (mm^2)	93 (± 18; 65−125)	88 (± 6; 80−97)
A1/B2	10%	11%
A2/B1	13%	13%
B2. Articular surface metacarpal head adduction-abduction (mm^2)	126 (± 24; 90−164)	125 (± 10; 109−136)
A1/B2	8%	8%
A2/B2	9%	10%
B3. Articular surface metacarpal head flexion-(hyper)extension (mm^2)	256 (± 23; 225−286)	235 (± 23; 199−276)
A1/B3	4%	4%
A2/B3	5%	5%
Volume		
C1. Countersunk portion of screw 2.4 (mm^3)	36 (± 5; 28−42)	33 (± 4; 27−39)
C2. Countersunk portion of screw 3.0 (mm^3)	43 (± 6; 34−52)	40 (± 5; 33−49)
D. Volume of metacarpal head (mm^3)	902 (± 123; 711−1,100)	686 (± 100; 466−801)
C1/D	4%	5%
C2/D	5%	6%
Range of engagement phalanx—countersunk		
E1. Start of flexion range center of phalanx base (until 90° flexion)	−16 (± 3; −13 to −20)	−15 (± 2; −13 to −18)
Total extension-flexion range (120°)	88%	88%
E2. Start of flexion range rim of phalanx base (until 90° flexion)	15 (± 5; 7−22)	13 (± 6; 6−22)
Total extension-flexion range (120°)	63%	64%